

Secondary defects of as-grown oxygen precipitates in nitrogen doped Czochralski single crystal silicon

Huan Tuo ^{a,b,1}, Yun Liu ^{a,1}, Minghao Li ^{a,c}, Rongwang Dai ^{a,c}, Hao Wang ^{a,c}, Yuehui Yu ^{a,c}, Zhongying Xue ^{a,c,*,}, Xing Wei ^{a,c,*}

^a State Key Laboratory of Functional Materials for Informatics, Shanghai Institute of Microsystem and Information Technology, Chinese Academy of Sciences, Shanghai, 200050, China

^b School of Physical Science and Technology, ShanghaiTech University, Shanghai, 201210, China

^c University of Chinese Academy of Sciences, Beijing, 100049, China



ARTICLE INFO

Keywords:

Secondary defects
as-grown oxygen precipitates
Nitrogen-doped
CZ silicon

ABSTRACT

In this work, as-grown defects and their secondary defects in 300 mm nitrogen-doped Czochralski-grown single-crystal silicon (NCZ-Si) are investigated. Secondary defects are revealed by homogeneous epitaxial layer growth, and as-grown defects are decorated via gaseous hydrogen chloride (HCl) etching. Localized light scattering (LLS) technique is utilized to inspect defect distribution and provide the latex sphere equivalent (LSE) size to differentiate defect types. With the locations of LLS, the morphology of defect is observed by scanning electron microscopy (SEM). According to the results, it indicated that secondary defects are extrinsic dislocation loops and stacking fault (SF) loops, which are induced by as-grown oxygen precipitates during the growth and cooling process. Furthermore, the correlation between the counts of secondary defects and nitrogen concentration is obtained. It contributes to the optimization of nitrogen doping to avoid the generation of detrimental defects for device operation.

1. Introduction

Single crystal silicon grown by Czochralski (CZ) method is widely used as substrates for advanced integrated circuits [1,2]. However, with the shrinking of feature size of integrated circuits, device failures caused by metal contamination and wafer warpage become more prominent. Therefore, higher gettering efficiency and mechanical strength are required in silicon substrates, which is used to manufacture epitaxial wafers for dynamic random-access memory (DRAM) or logic circuits. Nitrogen is the most common dopant used to improve these properties of silicon substrate [3]. It is considered that nitrogen can bind vacancies and oxygen to form complexes as N_2V_2 [4,5] and N_mO_n ($m, n > 1$) [6–9] during crystal growth. The N_2V_2 formation consumes considerable vacancies to suppress the formation of micro voids, i.e., crystal originated particles (COPs) formed by the aggregation of excess vacancies [10], which are beneficial to gate oxide integrity (GOI) [11,12]. In addition,

N_2V_2 combines oxygen atoms to form the $N_2V_2O_X$ complex at high temperatures [13,14]. N_mO_n and $N_2V_2O_X$ can act as heterogeneous nuclei to enhance oxygen precipitation [13,15]. It has been reported that nitrogen-doped CZ-Si has high-density oxygen precipitates (OPs) even after a high-temperature process [16,17]. Meanwhile, secondary defects such as dislocations and stacking faults (SFs) are probably induced by enhanced OPs, which increase the risk of device failure. It has been reported that rod-like COPs and OPs in the OISF ring are the cause of secondary defects [18,19]. However, as-grown defects outside the OISF ring are the potential troubles, which has been never investigated.

In this paper, homogeneous epitaxial growth and gaseous HCl etching [20] are applied to decorate secondary defects and as-grown defects in nitrogen-doped CZ-silicon (NCZ-Si) wafers, respectively. Localized light scattering (LLS) equipment is utilized to inspect defect distribution and provide the locations and latex sphere equivalent (LSE)

* Corresponding author. State Key Laboratory of Functional Materials for Informatics, Shanghai Institute of Microsystem and Information Technology, Chinese Academy of Sciences, Shanghai 200050, China.

** Corresponding author. State Key Laboratory of Functional Materials for Informatics, Shanghai Institute of Microsystem and Information Technology, Chinese Academy of Sciences, Shanghai 200050, China.

E-mail addresses: simsnow@mail.sim.ac.cn (Z. Xue), xwei@mail.sim.ac.cn (X. Wei).

¹ These authors contributed equally to this work and should be considered co-first authors.

sizes of defects. The types and morphologies of defects are determined by scanning electron microscopy (SEM). The formation mechanism of secondary defects is discussed. In addition, the relationship between the secondary defects and nitrogen concentration is elucidated. This work demonstrates that secondary defect formation can be prevented by optimizing the nitrogen concentration in the process of growing high-quality nitrogen-doped single-crystal silicon.

2. Experiment

Three batches of 300 mm NCZ-Si wafers obtained from three different segments of one Si ingot were used in this research. All the wafers are *p*-type (boron-doped, $8\text{--}12 \Omega\text{cm}$, $<100>$ orientation and thickness of 775 μm). The interstitial oxygen (O_i) concentrations of the NCZ-Si wafers were $5.0\text{--}5.5 \text{E+17 cm}^{-3}$, which are measured by Fourier transform infrared spectroscopy (FTIR) with a conversion factor of $3.14 \text{ E+17 cm}^{-2}$. The difference between these wafers is the nitrogen concentration (Nc). The Si ingot was doped with nitrogen by melting a Si₃N₄ layer-covered Si wafer in a crucible during crystal growth process. However, because of the difference in segregation coefficient (0.0007) between silicon melt and crystals [21], the Nc estimated by the segregation coefficient in the whole ingot varied from 0.7 E+14 cm^{-3} to 3.4 E+14 cm^{-3} along the ingot growth direction. In a narrow Si position, the Nc changed very little. Thus, for the three batches of 300 mm wafer obtained from different segments, their typical Nc values, including 7.57 E+13 , 1.18 E+14 and $3.23 \text{ E+14 cm}^{-3}$, are used as the nominated Nc.

After chemical mechanical polishing (CMP) and RCA cleaning, all the Si wafers were inspected by an LLS (The detection limit of LLS tool is about 15 nm) to record the initial surface irregularities, such as particles and pits. Then, these wafers were divided into three groups to implement different processes, the three groups were named Group I, II and III, respectively. Each group contains three wafers with different Ncs (7.57 E+13 , 1.18 E+14 and $3.23 \text{ E+14 cm}^{-3}$). It should be noted that these wafers with the same Nc in three Groups were adjacent to each other. Wafers in Group I were annealed at 1100 °C for 2 h under a wet oxidation condition to form oxidation-induced stacking faults (OISF). After that, X-ray topography (XRT) was used to observe the OISF rings in

wafers. A homogeneous epitaxial layer of 2.0 μm thickness was deposited on each wafer of Group II by CVD at a temperature above 1100 °C to reveal secondary defects. The wafers of Group III were etched by gaseous HCl for 40 s at 900 °C to decorate the as-grown defects. After finishing above processes, the LLS tool was applied again to obtain distribution of defects in Group II and III. Using the defect locations and latex sphere equivalent (LSE) sizes provided by the LLS tool, the morphologies of defects were identified and observed by scanning electron microscopy (SEM).

3. Results and discussion

Fig. 1 (a), (b) and (c) show the scanned results of defects on NCZ-Si substrates with the Ncs of 7.57 E+13 , 1.18 E+14 and $3.23 \text{ E+14 cm}^{-3}$, respectively. Only some process defects such as particles and scratches were identified by LLS after CMP and RCA cleaning. No COPs were observed on these wafers. Even after conducting OISF thermal treatment, OISF rings were not observed by XRT mapping on Group I wafers, as shown in **Fig. 1** (d), (e) and (f), which proved the NCZ-Si wafers in this work were COP-free and OISF-free.

The purpose of homoepitaxial growth is to provide a defect-free layer for device fabrication. However, some imperfections in the crystal lattice, such as dislocations, will propagate from substrate to epitaxial layer during homoepitaxial growth process, which is detrimental to the device. Thus, it is necessary to evaluate the effect of Nc on homoepitaxial growth. **Fig. 2** shows the LLS defect distributions of Group II wafers after homoepitaxial growth. It can be found that the density of epitaxial defects increases with nitrogen concentration. Compared with LLS maps of the substrate, the density of epitaxial defects was much higher than that of processing defects. Therefore, the formation of these epitaxial defects is not related to the process defects on the substrate surface.

As shown in **Fig. 3**, LSE size analysis is applied to identify these epitaxial defects. Samples with Ncs of $7.57 \text{ E+13 cm}^{-3}$, $1.18 \text{ E+14 cm}^{-3}$ and $3.23 \text{ E+14 cm}^{-3}$ have the same LSE size peak at 0.064 μm . It is also found that the size limit at Ncs with $7.57 \text{ E+13 cm}^{-3}$ and $1.18 \text{ E+14 cm}^{-3}$ is up to 0.068 μm , respectively. As the LSE size is associated with the morphology and scale of defects and LSE sizes greater than 0.068 μm are only found in wafers with Nc of $3.23 \text{ E+14 cm}^{-3}$, two ranges, Range-

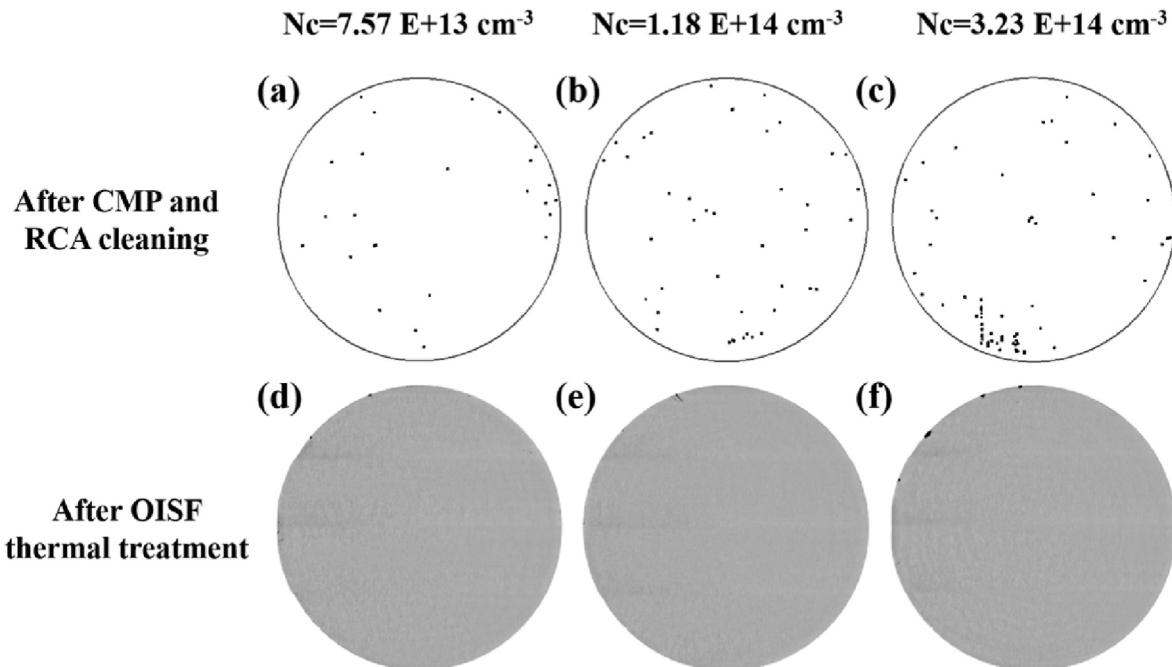


Fig. 1. (a) ~ (c) LLS scanned results of NCZ-Si wafers with Nc of 7.57 E+13 , 1.18 E+14 and $3.23 \text{ E+14 cm}^{-3}$, (d) ~ (f) XRT scanned results of NCZ-Si wafers after thermal treatment.

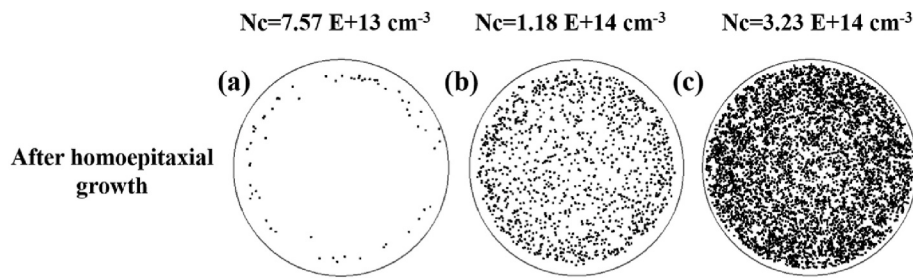


Fig. 2. LLS scanned results of the wafers after homoepitaxial growth with N_c of (a) $7.57 \text{ E}+13 \text{ cm}^{-3}$, (b) $1.18\text{E}+14 \text{ cm}^{-3}$ and (c) $3.23 \text{ E}+14 \text{ cm}^{-3}$.

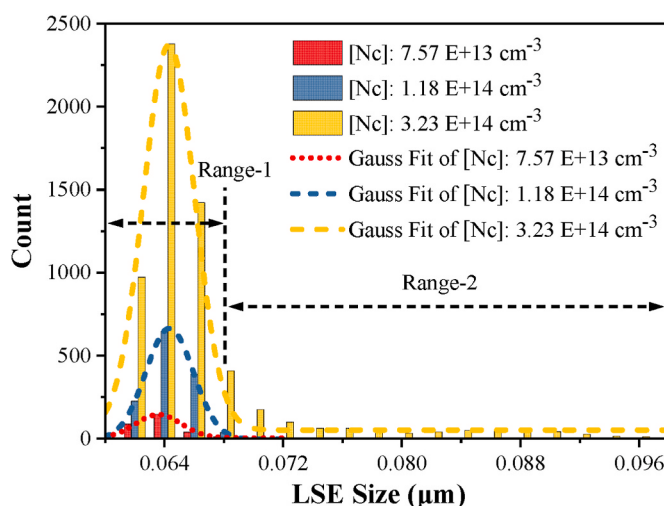


Fig. 3. LSE size distribution of epitaxial defects from Group II wafers with the N_c of $7.57 \text{ E}+13 \text{ cm}^{-3}$, $1.18 \text{ E}+14 \text{ cm}^{-3}$ and $3.23 \text{ E}+14 \text{ cm}^{-3}$.

1 and -2, were divided with a boundary size of $0.068 \mu\text{m}$. It is further inferred that Range-1 and -2 likely represent different types of epitaxial defects.

With the locations and LSE sizes of defects in Range-1 and -2 identified by LLS, SEM is utilized to investigate their origination. The SEM detector receives secondary electrons (SE) from the $[1\bar{1}0]$ direction shown in Fig. 4. According to the images, there are two main types of defects in Group II. The first defect type is “dimple” presented in Range-1, as shown in Fig. 4 (a), (b) and (c). It is well known that the dislocation stress is proportional to $1/r$, where r is the distance from the dislocation center. Thus, the Si deposition rate at dislocation should be higher than at other locations. However, surface atoms near dislocation will migrate out due to high strain energy at very high temperatures during epitaxial growth. Therefore, the dimples are considered as dislocations. What's more, the pair formed of dimples indicates that they are truncated dislocation loops.

The other type of epitaxial defect in Range-2 is the straight trench along the $[110]$ direction, as shown in Fig. 4 (d), (e) and (f). The morphology is typical SF in epitaxial layer. These figures indicate that the LSE size is related to SF length. It is known that the SF plane is $\{111\}$ in the monocrystalline silicon structure. If SF propagate along intersectant $<110>$ direction, like inverted triangle, the length of SF can be calculated by $2 h/\tan\theta$, where h is the height from origin to surface, θ is the angle between plane $\{100\}$ and $\{111\}$, i.e., 54.7° . If SF is generated

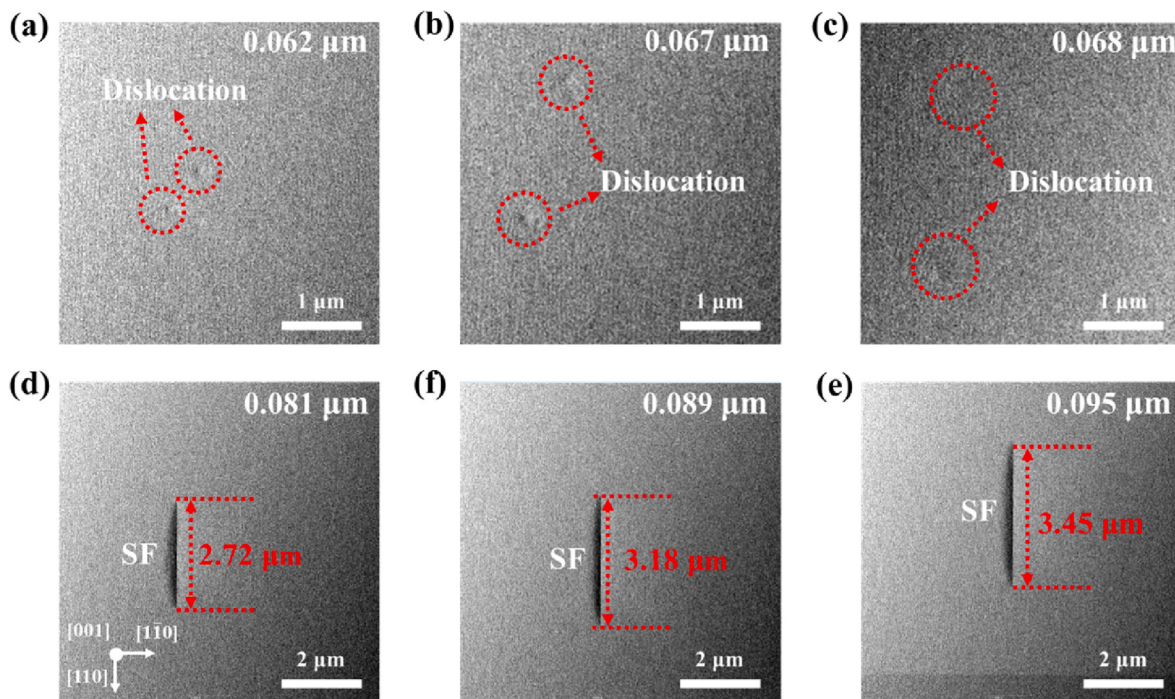


Fig. 4. SEM images of epitaxial defects with different LSE sizes, (a) ~ (c) dislocations in Range-1, (d) ~ (f) SFs in Range -2. The value indicated on top right corner of each image shows the LSE size.

from the interface between the epitaxial layer and the Si substrate, h is equal to the epitaxial thickness and thus the SF length is about 2.83 μm . However, according to SEM observations, the SF lengths deviate from 2.83 μm randomly, as shown in Fig. 4 (d), (e) and (f). The longer SF implies that the origin is beneath substrate. Therefore, the propagation direction of SFs is not along intersectant $<110>$ direction, otherwise, SFs will be throughout the whole ingot. Considering the shorter SFs, it is inferred that the propagation direction of SFs should be parallel $<110>$ and SFs should be closed.

To investigate the origin and characteristics of defects in the epitaxial layer, two samples were subjected to FIB cutting along the direction indicated in Fig. 5 (a), and the “dimple” were identified as dislocations, as shown in Fig. 5 (b). A single dislocation was observed in the image, but not a loop, which can be explained by the fact that the dislocation loop does not lie entirely on a specific crystal plane. Therefore, the TEM results in this work only revealed a segment of the dislocation loop. Moreover, Fig. 5 (c) and (d) showed that the straight trench is a stacking fault, which is situated on the $\{111\}$ plane and propagated into the epitaxial layer from the substrate along the $<110>$ direction. TEM observations indicated that the defects in the epitaxial layer consist of dislocations and stacking faults, which were caused by the as-grown defects in the substrates rather than the substrate surface.

Gaseous HCl etching is an effective method to reveal as-grown defects in NCZ-Si wafers, which will help to investigate the origins of epitaxial defects. Fig. 6 shows LLS mappings of defects after HCl etching for 40 s in Group III. Defect counts increases significantly with the increase of Nc. It is also found that the radial density variation of etched wafers is similar to that of epitaxial wafers. Similarly, we analyzed the LSE size distribution of the etched defects, as shown in Fig. 7. According to the Gauss fit curves, two peaks at 0.048 and 0.056 μm were observed and they have an intersection LSE size at 0.052 μm . Meanwhile, defects of LSE size greater than 0.064 μm are only found at Nc of 3.23 E+14

cm^{-3} . Thus, three ranges, i.e., Range-3, -4 and -5 are divided according to LSE size variation. The boundary between Range-3 and Range-4 is the junction of two peak, i.e., 0.052 μm . Range-5 is isolated since it only occurs at Nc of 3.23 E+14 cm^{-3} . It is also inferred that Range-3, -4 and -5 likely represent different morphologies of etched defects.

SEM method is used to observe the defect morphologies again with the locations of LLS, as shown in Fig. 8 and Fig. 9. There are three types of defects in the etched samples. The first defect type in Range-3 is the etch pit with a core in the center, as shown in Fig. 8 (a). The central core in the pit is identified as as-grown OP by SEM energy dispersive X-ray (SEM-EDX) spectrum analysis, due to the present of oxygen peak, as shown in Fig. 8 (b). Compared with the LLS results obtained from as-grown wafers (Fig.), it is believed that the NCZ-Si wafers in this work are Pv (pure vacancy) region [22]. The Pv region between the P-band (OISF region) and the V/I boundary is characterized by the mutual annihilation of vacancies and interstitials, resulting in insufficient vacancy concentrations to form any observable microdefects such as COPs or OISF ring. In addition, in the Pv region, as-grown OPs are too small to be detected before implementing HCL etch. The type of defects in Range-4 is a pair of “inverted pyramid” pits shown in Fig. 9 (a) and (b). It is known that the etching rate decreases from the center of the dislocations outward due to the presence of the strain field. Therefore, defects in Range -4 are considered to be dislocation loops, which could propagate from the substrate to the epitaxial layer leading to epitaxial dislocations. Moreover, as shown in Fig. 9 (c) and (d), a row of “inverted pyramid” pits along the $[110]$ direction was observed in Range-5. Their lengths were similar to that of epitaxial SFs. Defects in Range -5 were considered to be extrinsic (interstitial type) faulted loops lying on $\{111\}$ planes with Frank-type partial dislocations. It is well known that the formation of extrinsic dislocation loops and SF loops are associated with the aggregation of self-interstitials. During the growth of OPs, a large number of interstitials are emitted to release the stress, and aggregate

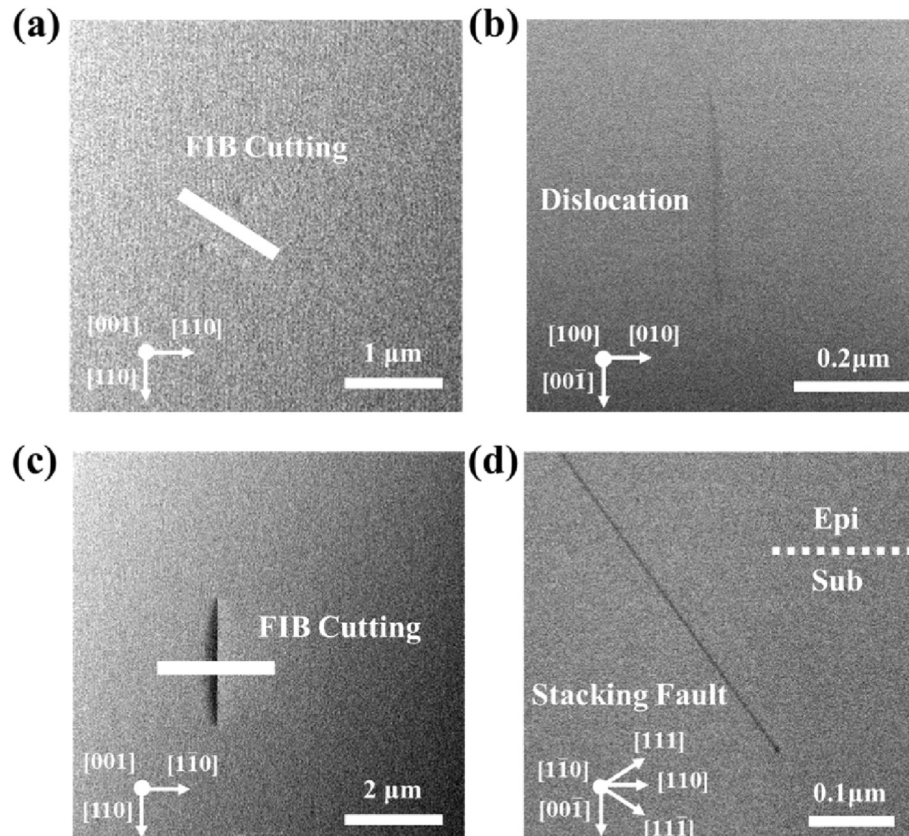


Fig. 5. Cross-sectional TEM observations of defects in epitaxial layer, (a) and (b) “dimples (dislocation)”, (c) and (d) “straight trench (stacking fault)”.

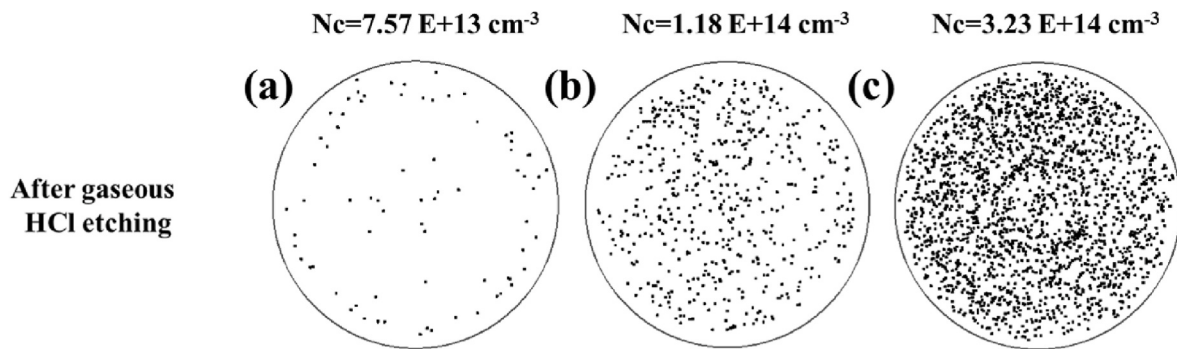


Fig. 6. LLS scanned results of as-grown defects on wafers of Group III after 40 s HCl etching, (a) $N_c = 7.57 \text{ E}+13 \text{ cm}^{-3}$, (b) $N_c = 1.18 \text{ E}+14 \text{ cm}^{-3}$ and (c) $N_c = 3.23 \text{ E}+14 \text{ cm}^{-3}$.

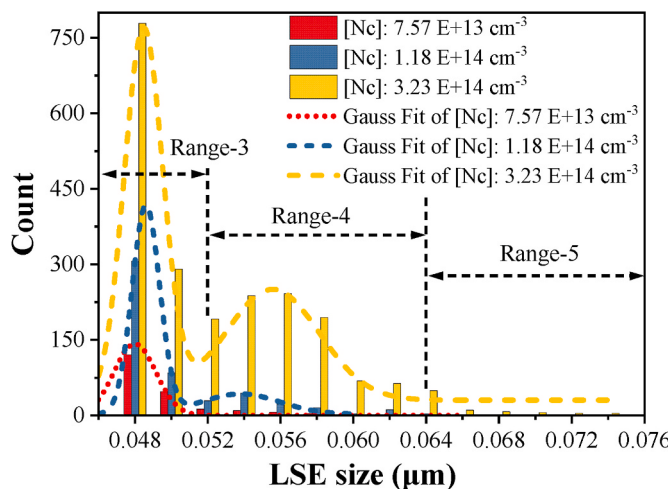


Fig. 7. LSE size distribution of as-grown defects on the etched wafers with N_c of $7.57 \text{ E}+13$, $1.18 \text{ E}+14$ and $3.23 \text{ E}+14 \text{ cm}^{-3}$.

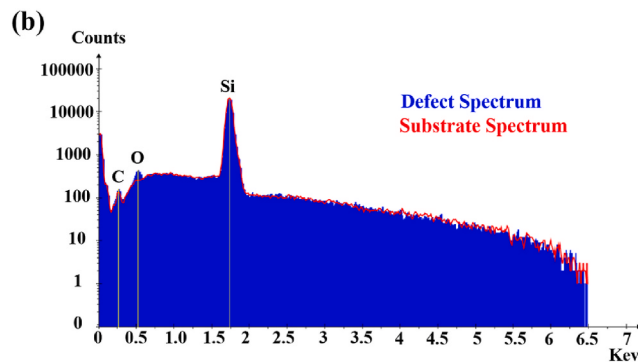
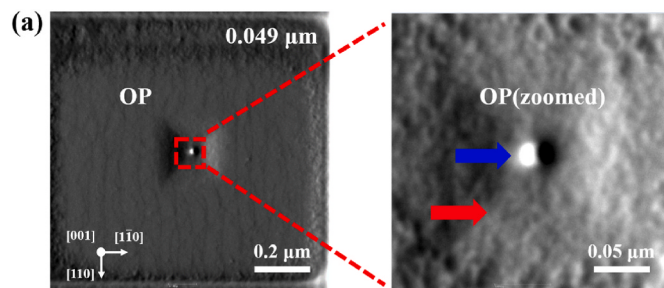


Fig. 8. (a) SEM images of as-grown OP in Range-3, (b) SEM-EDX analysis of center defect (blue arrow) and substrate (red arrow) in the etch pit.

around OPs to form secondary defects, i.e., dislocation and SF. It usually occurs in OISF ring due to the large size of OPs after thermal treatment. However, nitrogen have a stronger enhancement effect on oxygen precipitation compared to previous reports, so that as-grown OPs in Pv region are enhanced to induce secondary defects.

According to the above results and discussions, different N_c results in different counts and type of secondary defect. Therefore, the control of N_c is necessary for the manufacture of high-quality NCZ-Si substrates. To investigate the effect of N_c on the amounts of secondary defects quantitatively, more experimental data were collected. The high correlativity of logarithmic curve fitting in Fig. 10 indicates that the number of secondary defects increase logarithmically with the N_c . Two N_c thresholds are found to generate dislocations and SFs, i.e., approximately $5.5 \text{ E}+13 \text{ cm}^{-3}$ and $1.7 \text{ E}+14 \text{ cm}^{-3}$, respectively. This result contributes to the optimization of nitrogen doping to avoid the generation of secondary defects.

4. Conclusion

The N_c dependence on as-grown and secondary defects was investigated using NCZ-Si wafers. After homoepitaxial growth, dimples in pairs and straight trenches in epitaxial layers were found by SEM images. They are divided with the LSE size boundary of $0.068 \mu\text{m}$ identified by the LLS tool. The dimple in pairs and straight trenches are classified as dislocation loops and SFs. It has been indicated that the SFs could propagate from the substrate to the epitaxial layer parallel $<110>$ direction and SFs should be closed. After gaseous HCl etching, three types of defects including OPs, dislocations and SFs are found. The defect region of NCZ-Si wafers is confirmed as Pv region. It is indicated that secondary defects are induced by enhanced OPs and the enhancement effect on OPs is related to N_c . In addition, a logarithmic fit of the N_c -dependent effect on the number of secondary defects is plotted. Two N_c thresholds of approximately $5.5 \text{ E}+13 \text{ cm}^{-3}$ and $1.7 \text{ E}+14 \text{ cm}^{-3}$ were found to avoid dislocation loops and closed SFs generation. It is of great significance to avoid the formation of detrimental defects in NCZ-Si wafers for improving device yields.

CRediT authorship contribution statement

Huan Tuo: Writing – original draft, Investigation. **Yun Liu:** Writing – original draft, Investigation. **Minghao Li:** Investigation. **Rongwang Dai:** Investigation. **Hao Wang:** Investigation. **Yuehui Yu:** Investigation. **Zhongying Xue:** Writing – review & editing, Supervision, Project administration, Conceptualization. **Xing Wei:** Writing – review & editing, Supervision, Project administration, Conceptualization.

Declaration of competing interest

The authors declare that they have no known competing financial

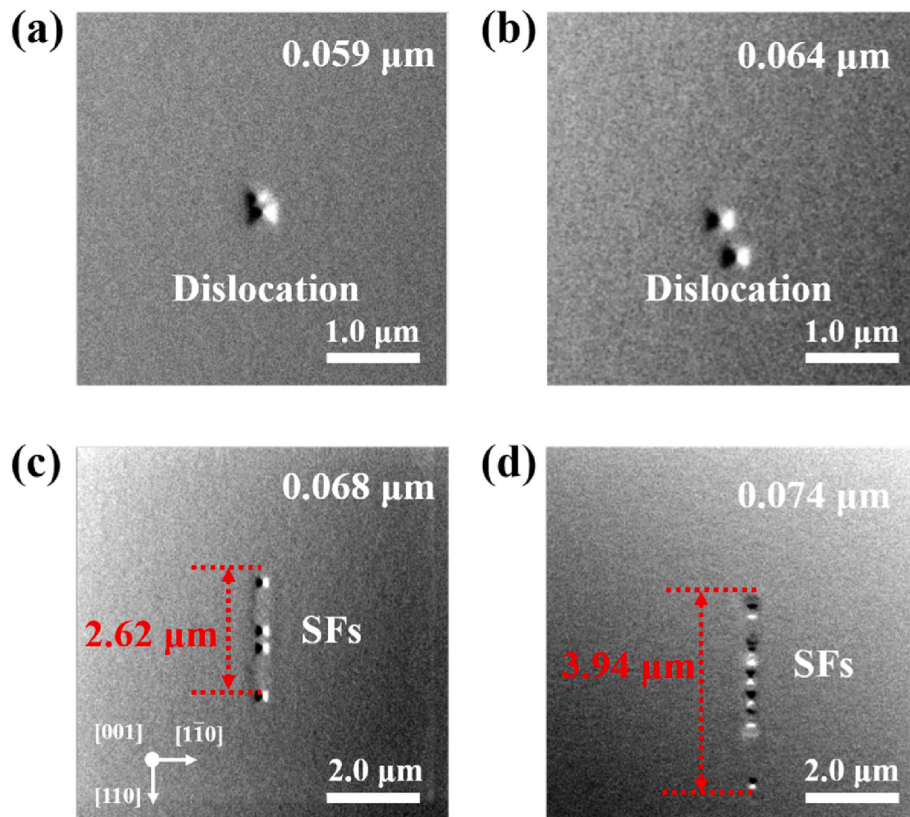


Fig. 9. SEM images of etched defects with different LSE sizes, (a) and (b) show dislocation in Range-4, (c) and (d) show SFs in Range-5.

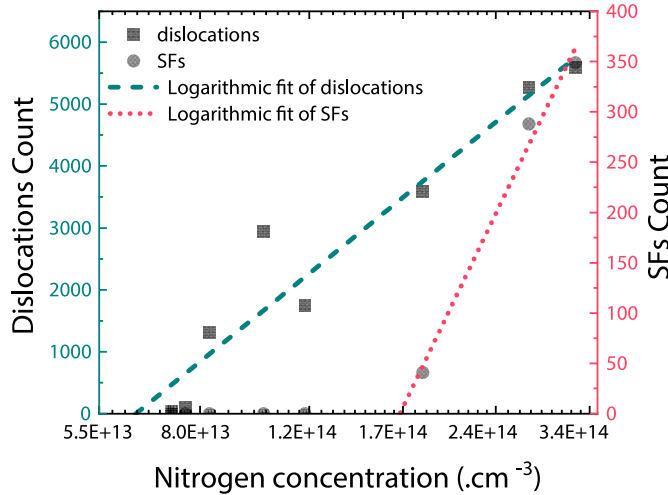


Fig. 10. The Nc-dependence effect on the number of dislocations and SFs.

interests or personal relationships that could have appeared to influence the work reported in this paper.

Data availability

Data will be made available on request.

Acknowledgments

This work was financially supported by National Natural Science Foundation of China under Grant No. 62074152 and Shanghai Science and Technology Development Foundation under Grant No.

23YF1456100.

References

- [1] A. Ikari, K. Nakai, Y. Tachikawa, H. Deai, Y. Hideki, Y. Ohta, N. Masahashi, S. Hayashi, T. Hoshino, W. Ohashi, Defect control in nitrogen doped Czochralski silicon crystals, Solid State Phenomena, Trans Tech Publ (1999) 161–166. <http://doi.org/10.4028/www.scientific.net/SSP.69-70.161>.
- [2] E. Dornberger, D. Temmler, W. Von Ammon, Defects in silicon crystals and their impact on DRAM device characteristics, J. Electrochem. Soc. 149 (4) (2002) G226, <https://doi.org/10.1149/1.1454141>.
- [3] F. Shimura, R. Hockett, Nitrogen effect on oxygen precipitation in Czochralski silicon, Appl. Phys. Lett. 48 (3) (1986) 224–226, <https://doi.org/10.1063/1.96564>.
- [4] J.P. Goss, I. Hahn, R. Jones, P.R. Briddon, S. Oberg, Vibrational modes and electronic properties of nitrogen defects in silicon, Phys. Rev. B 67 (4) (2003), 045206, <https://doi.org/10.1103/PhysRevB.67.045206>.
- [5] H. Sawada, K. Kawakami, First-principles calculation of the interaction between nitrogen atoms and vacancies in silicon, Phys. Rev. B 62 (3) (2000) 1851–1858, <https://doi.org/10.1103/PhysRevB.62.1851>.
- [6] M. Suezawa, K. Sumino, H. Harada, T. Abe, The nature of nitrogen-oxygen complexes in silicon, Jpn. J. Appl. Phys. 27 (1R) (1988) 62, <https://doi.org/10.1143/JJAP.27.62>.
- [7] D. Yang, D. Que, K. Sumino, Nitrogen effects on thermal donor and shallow thermal donor in silicon, J. Appl. Phys. 77 (2) (1995) 943–944, <https://doi.org/10.1063/1.359024>.
- [8] D.R. Yang, R.X. Fan, L.B. Li, D.L. Que, K. Sumino, Effect of nitrogen-oxygen complex on electrical properties of Czochralski silicon, Appl. Phys. Lett. 68 (4) (1996) 487–489, <https://doi.org/10.1063/1.116422>.
- [9] A. Karoui, F.S. Karoui, A. Kvít, G. Rozgonyi, D. Yang, Role of nitrogen related complexes in the formation of defects in silicon, Appl. Phys. Lett. 80 (12) (2002) 2114–2116, <https://doi.org/10.1063/1.1462874>.
- [10] J. Ryuta, E. Morita, T. Tanaka, Y. Shimanuki, Crystal-originated singularities on Si wafer surface after ScI cleaning, Japanese Journal of Applied Physics Part 2-Letters & Express Letters 29 (11) (1990) L1947–L1949, <https://doi.org/10.1143/JJap.29.L1947>.
- [11] W. Ammon, P. Dreier, W. Hensel, U. Lambert, L. Köster, Influence of oxygen and nitrogen on point defect aggregation in silicon single crystals, Mater. Sci. Eng., B 36 (1–3) (1996) 33–41, [https://doi.org/10.1016/0921-5107\(95\)01295-8](https://doi.org/10.1016/0921-5107(95)01295-8).
- [12] H. Kageshima, A. Taguchi, K. Wada, Theoretical investigation of nitrogen-doping effect on vacancy aggregation processes in Si, Appl. Phys. Lett. 76 (25) (2000) 3718–3720, <https://doi.org/10.1063/1.126760>.

- [13] H. Kageshima, A. Taguchi, K. Wada, Formation of stable N-V-O complexes in Si, Phys. B Condens. Matter 340 (2003) 626–629, <https://doi.org/10.1016/j.physb.2003.09.121>.
- [14] A. Taguchi, H. Kageshima, K. Wada, First-principles investigations of nitrogen-doping effects on defect aggregation processes in Czochralski Si, J. Appl. Phys. 97 (5) (2005), 053514, <https://doi.org/10.1063/1.1858057>.
- [15] A. Karoui, F.S. Karoui, G.A. Rozgonyi, M. Hourai, K. Sueoka, Structure, energetics, and thermal stability of nitrogen-vacancy-related defects in nitrogen doped silicon, J. Electrochem. Soc. 150 (12) (2003) G771–G777, <https://doi.org/10.1149/1.1621418>.
- [16] K. Nakai, Y. Inoue, H. Yokota, A. Ikari, J. Takahashi, A. Tachikawa, K. Kitahara, Y. Ohta, W. Ohashi, Oxygen precipitation in nitrogen-doped Czochralski-grown silicon crystals, J. Appl. Phys. 89 (8) (2001) 4301–4309, <https://doi.org/10.1063/1.1356425>.
- [17] X. Yu, D. Yang, X. Ma, J. Yang, L. Li, D. Que, Grown-in defects in nitrogen-doped Czochralski silicon, J. Appl. Phys. 92 (1) (2002) 188–194, <https://doi.org/10.1063/1.1481190>.
- [18] K. Nakai, K. Kitahara, Y. Ohta, A. Ikari, M. Tanaka, Crystal defects in epitaxial layer on nitrogen-doped Czochralski-grown silicon substrate (I) - investigation of the crystallographic structure, Japanese Journal of Applied Physics Part 1-Regular Papers Short Notes & Review Papers 43 (4a) (2004) 1241–1246, <https://doi.org/10.1143/Jjap.43.1241>.
- [19] K. Nakai, K. Kitahara, Y. Ohta, A. Ikari, M. Tanaka, Crystal defects in epitaxial layer on nitrogen-doped czochralski-grown silicon substrate (II) - suppression of the crystal defects in epitaxial layer by the control of crystal growth condition and carbon co-doping, Japanese Journal of Applied Physics Part 1-Regular Papers Short Notes & Review Papers 43 (4a) (2004) 1247–1253, <https://doi.org/10.1143/Jjap.43.1247>.
- [20] Y. Liu, T. Wei, M. Li, Z. Li, Z. Xue, X. Wei, Characterization of grown-in defects in Si wafers by gas decoration, Mater. Sci. Semicond. Process. 130 (2021), 105822, <https://doi.org/10.1016/j.mssp.2021.105822>.
- [21] Y. Yatsurugi, N. Akiyama, Y. Endo, T. Nozaki, Concentration, solubility, and equilibrium distribution coefficient of nitrogen and oxygen in semiconductor silicon, J. Electrochem. Soc. 120 (7) (1973) 975, <https://doi.org/10.1149/1.2403610>.
- [22] G. Kissinger, Oxygen impurity in crystalline silicon, Handbook of Photovoltaic Silicon (2019) 399–436, https://doi.org/10.1007/978-3-662-56472-1_20.